Optical detection of x-ray-absorption spectra: Sodium salicylate as an example

D. B. M. Klaassen
Philips Research Laboratories, P.O. Box 80000, 5600 JA Eindhoven, The Netherlands
(Received 11 April 1988)

In the optical detection of extended x-ray-absorption fine structure (EXAFS), x-ray radiation is absorbed, followed by the generation of "intermediate" electron-hole pairs. These *e-h* pairs may excite luminescent centers or recombine radiatively. The optical radiation produced upon decay of excited luminescent centers or radiative recombination of *e-h* pairs is detected. In the interpretation of the optical detection of EXAFS only the scattering and absorption of exciting x rays and generated light have hitherto been considered. This paper discusses the effect of diffusion of the intermediate *e-h* pairs to the surface of a single crystal or powder grains followed by radiationless recombination. The theory developed here is used to eliminate an apparent inconsistency between published measurements on the efficiency of sodium salicylate.

I. INTRODUCTION

The correspondence between x-ray absorption and uv luminescence excitation spectra was observed for the first time by Bianconi *et al.*[1] for calcium fluoride in the region of the K edge of calcium. From this correspondence the method of measuring extended x-ray-absorption fine structure (EXAFS) spectra via optical luminescence was developed.[2–5]

By analogy with the interpretation of x-ray fluorescence detection of EXAFS (Ref. 6) only absorption and scattering of both exciting x rays and generated radiation are considered in the interpretation of the detection of EXAFS by optical (uv, visible) luminescence.[2,3] Diffusion of the "intermediate"[7] electron-hole pairs to the surface followed by nonradiative recombination is neglected.

Within the framework of the existing interpretation there is a discrepancy between published experiments. Bianconi *et al.*[1] found a negative edge in the optical luminescence excitation spectrum of monocrystalline calcium fluoride at the K edge of calcium, whereas Goulon *et al.*[4] found a positive edge for a powdered sample. The negative edge found by Bianconi *et al.* was 4%.[1] Recently we found negative edges of 25–50 % in the visible luminescence excitation spectra of lanthanide oxysulphides, which were activated with terbium or europium, at the positions of the giant $4d \rightarrow 4f$ resonances of the lanthanide atoms.[8] In this energy region the penetration depth of the soft x rays is of the same order of magnitude as the diffusion length of the *e-h* pairs. Therefore in the interpretation of these experiments the diffusion of intermediate *e-h* pairs to the surface followed by radiationless recombination had to be taken into account.

The effect of diffusion of intermediate *e-h* pairs to the surface followed by radiationless recombination was discussed by Elango *et al.*[9] for monocrystalline samples. For powder samples, however, scattering and absorption of the optical luminescence have to be taken into account as well. This paper presents a calculation of the combined influence of both effects on the efficiency and sensitivity of optically detected EXAFS. The appearance of positive and negative edges in EXAFS spectra is discussed.

In the soft-x-ray region the visible scintillator sodium salicylate is often used as a photon-flux monitor. As surface recombination of *e-h* pairs is especially important in this energy region,[8] it affects the external efficiency of sodium salicylate. Recent publications report widely different values for the efficiency of sodium salicylate in the energy region between 100 and 250 eV.[9–11] The theory developed here is used to eliminate this apparent inconsistency.

II. THEORY

A. Introduction

At the beginning of this section a few remarks should be made. For both scattering and absorption of radiation as well as diffusion of electron-hole pairs in powder samples no simple formulations treating these problems in their complete three-dimensional sophistication are available. However, quite simple one-dimensional theories for both problems have been published, which have been well tested and which incorporate all the major features required for treating the problem at hand.

Using these one-dimensional theories it is still not possible, however, to derive analytical expressions for the efficiency and sensitivity of the optical detection of EXAFS. As numerical techniques using a computer are inevitable, only the differential equations, the form of the general solutions, and boundary conditions are given.

B. Generation and diffusion of *e-h* pairs

The density of generated electron-hole pairs $n(x)$ at a distance x from the (irradiated) front surface of the sample is given by the differential equation[12]

$$\frac{d^2n}{dx^2}=\frac{n}{L^2}-\frac{\mu\mathcal{I}\tau}{L^2}e^{-\mu x} . \tag{1}$$

The general solution is

$$n(x)=C_1e^{-x/L}+C_2e^{x/L}+C_3e^{-\mu x} . \tag{2}$$

Here L is the diffusion length of the e-h pairs, μ is the absorption coefficient of the x rays, τ is the volume lifetime of the e-h pairs, $\mathcal{J}$ is the flux of the incident x-ray radiation, and C_3 is given by

$$C_3=\frac{\mu\mathcal{J}\tau}{1-\mu^2L^2} . \tag{3}$$

The constants C_1 and C_2 are determined by the following boundary conditions: At the front surface of the sample,

$$D\left[\frac{dn}{dx}\right]=Sn ; \tag{4a}$$

at the back surface of the sample,

$$D\left[\frac{dn}{dx}\right]=-Sn , \tag{4b}$$

where D is the diffusion constant and S is the surface recombination velocity of the e-h pairs. For powder samples these boundary conditions have to be satisfied at every grain. This implies that for powder samples we get a separate solution of the form of Eq. (2) for each grain. Expressions for C_1 and C_2 can be found in Appendix A.

C. Generation and scattering of optical luminescence

The scattering of the optical luminescence is described with the differential equations formulated by Kubelka and Munk[13] and extended with a light-generation profile $P(x)$ by Hamaker:[14]

$$\frac{dI}{dx}=-(r+s)I+rJ+\frac{P}{2} \tag{5}$$

and

$$\frac{dJ}{dx}=(r+s)J-rI-\frac{P}{2} , \tag{6}$$

where I and J are the light fluxes in the direction of the positive and negative x axis, respectively; s is the absorption constant and r is the scattering (or remission) constant. The light generation profile is proportional to the density of e-h pairs. Neglecting the volume nonradiative recombination of e-h pairs we have

$$P(x)=\frac{n(x)}{\tau} . \tag{7}$$

The solutions of Eqs. (5) and (6) are given by

$$I(x)=I_+e^{\alpha x}+I_-e^{-\alpha x}+I_1e^{-xL}+I_2e^{x/L}+I_3e^{-\mu x} \tag{8}$$

and

$$J(x)=J_+e^{\alpha x}+J_-e^{-\alpha x}+J_1e^{-x/L}+J_2e^{x/L}+J_3e^{-\mu x}, \tag{9}$$

where α is given by

$$\alpha=\sqrt{s(2r+s)} . \tag{10}$$

Substitution of Eqs. (8) and (9) in Eq. (5) yields the following relations:

$$I_+=H_\infty J_+ \tag{11}$$

and

$$H_\infty I_-=J_- , \tag{12}$$

where H_∞, the reflection coefficient of a semi-infinitely thick sample, is given by

$$H_\infty=\frac{r+s-\alpha}{r} . \tag{13}$$

Expressions for the coefficients I_i in Eq. (8) and J_i in Eq. (9) are given in Appendix B. The constants I_+ and I_- are determined by the boundary conditions: At the front surface of the sample,

$$I^{\text{front}}=0 , \tag{14}$$

at the back surface of the sample,

$$J^{\text{back}}=0 , \tag{15}$$

and at the boundary of grain k and grain $k+1$,

$$I^k=I^{k+1} , \tag{16a}$$

$$J^k=J^{k+1} . \tag{16b}$$

Thus for a layer which is N grains thick we have $2N$ equations with the same number of unknown coefficients. These equations can easily be solved numerically on a computer by writing them in the form of a matrix and using a matrix inversion routine. The optical flux from the sample in the reflection mode is then J^{front}, while the optical flux in the transmission mode equals I^{back}.

D. Efficiency and sensitivity

The efficiency of the detection process is defined as the ratio of optical flux from the sample and incident x-ray flux $\mathcal{J}$ on the sample, i.e., in the reflection mode

$$\eta_{\text{refl}}=\frac{J^{\text{front}}}{\mathcal{J}} \tag{17}$$

and in the transmission mode

$$\eta_{\text{trans}}=\frac{I^{\text{back}}}{\mathcal{J}} . \tag{18}$$

But rather than the efficiency of the process, it is of interest whether for instance, a positive edge in the x-ray absorption is detected as a positive or as a negative edge in the optical luminescence spectrum. Therefore we define the sensitivity of the detection process as

$$\chi=\frac{\mu}{\eta}\frac{d\eta}{d\mu} . \tag{19}$$

This sensitivity gives the factor between the magnitude of an edge in the optical luminescence spectrum and the corresponding edge in the x-ray absorption. Moreover, if the sensivity is positive, an edge in the x-ray absorption is detected as a positive edge, and if the sensitivity is negative, an edge in the x-ray absorption is detected as a negative edge in the optical luminescence spectrum.

III. RESULTS AND DISCUSSION

A. Efficiency and sensitivity of EXAFS

In order to get realistic results from the calculations an educated guess for the absorption coefficient s and the scattering coefficient r of the powder layer has to be made. From the literature $s=1$ cm^{-1} and $r=180$ cm^{-1} seem to be realistic values.[15] The resulting value for α is 19 cm^{-1} and the value found for H_∞ is 0.9. For the diffusion length of the e-h pairs we used 0.2 μm and a realistic value for the reduced surface recombination velocity S^* is 5 (see Appendix A and Refs. 8 and 9). The diameter of the grains is taken to be 5 μm.

The results for a thick powder layer with a thickness of 0.2 cm are presented in Fig. 1. From the efficiency we see that (as expected) for a thick layer only the reflection mode makes sense. From the sensitivity it can be seen that for absorption coefficients larger than 2×10^3 cm^{-1}, positive edges in the absorption are detected as negative edges in the optical luminescence. This value of 2×10^3 cm^{-1} corresponds to the inverse grain diameter. The results for a thin powder layer with a thickness of 50 μm are given in Fig. 2. From this figure we see that for thin layers this crossover point is shifted, due to light scattering, to larger absorption coefficients for the reflection mode, whereas it is reached at a smaller value for the transmission mode. So in contrast to the predictions of Goulon *et al.*[4] in both reflection and transmission modes positive and negative edges are to be encountered.

The absorption coefficient of CaF_2 at the K edge of Ca is of the order of 10^3 cm^{-1}.[16] From Fig. 1 it can be seen that the positive edge found for a thick powder sample of CaF_2 (in the reflection mode) by Goulon *et al.*[4] is in agreement with our model calculations. In order to perform a calculation for a monocrystalline sample the relations given in Secs. II C and II D have to be slightly changed (see Appendix C). From the results of our model calculation presented in Fig. 3, one can see that only

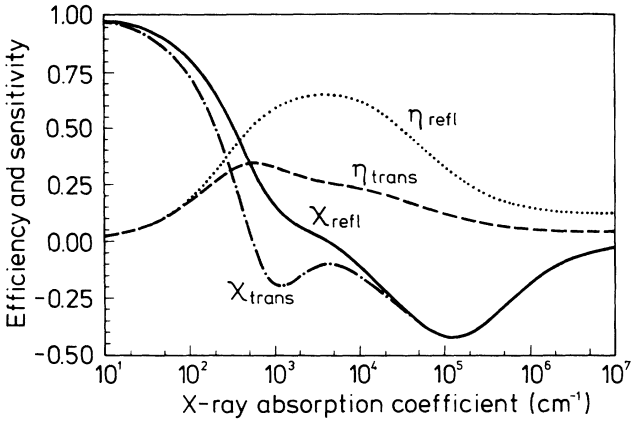

FIG. 2. Efficiency (dotted line for the reflection and dashed line for the transmission mode) and sensitivity (solid line for the reflection and dashed-dotted line for the transmission mode) for a thin powder layer as a function of the absorption coefficient μ of the exciting x rays. Layer thickness is 50 μm; grain diameter is 5 μm; absorption coefficient s is 1 cm^{-1}; and the scattering coefficient r is 180 cm^{-1}, resulting in α equal to 19 cm^{-1} and H_∞ equal to 0.9. The diffusion length of the e-h pairs is taken to be 0.2 μm and the reduced surface recombination velocity S^* is 5.

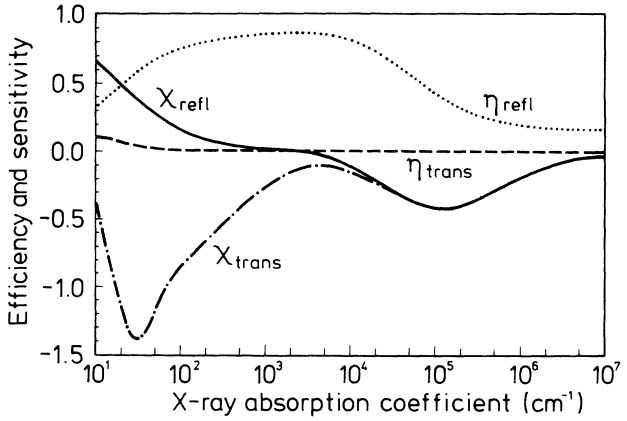

FIG. 1. Efficiency (dotted line for the reflection and dashed line for the transmission mode) and sensitivity (solid line for the reflection and dashed-dotted line for the transmission mode) for a thick powder layer as a function of the absorption coefficient μ of the exciting x rays. Layer thickness is 0.2 cm; grain diameter is 5 μm; absorption coefficient s is 1 cm^{-1} and the scattering coefficient r is 180 cm^{-1}, resulting in α equal to 19 cm^{-1} and H_∞ equal to 0.9. The diffusion length of the e-h pairs is taken to be 0.2 μm and the reduced surface recombination velocity S^* is 5.

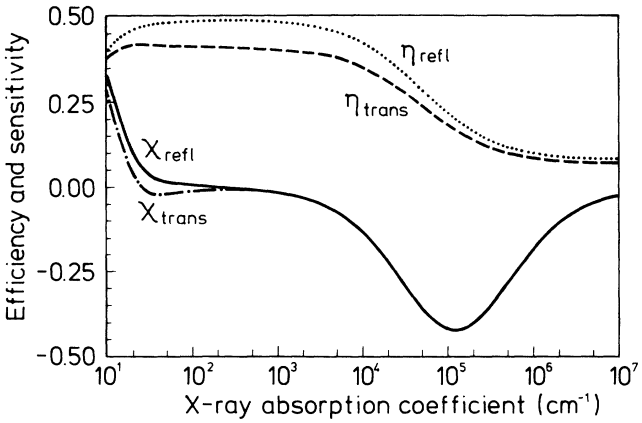

FIG. 3. Efficiency (dotted line for the reflection and dashed line for the transmission mode) and sensitivity (solid line for the reflection and dashed-dotted line for the transmission mode) for a monocrystalline sample as a function of the absorption coefficient μ of the exciting x rays. Sample thickness is 0.2 cm; absorption coefficient s is 1 cm^{-1}, resulting in α equal to 1 cm^{-1}; the reflection coefficient R is taken to be 0.05. The diffusion length of the e-h pairs is taken to be 0.2 μm and the reduced surface recombination velocity S^* is 5.

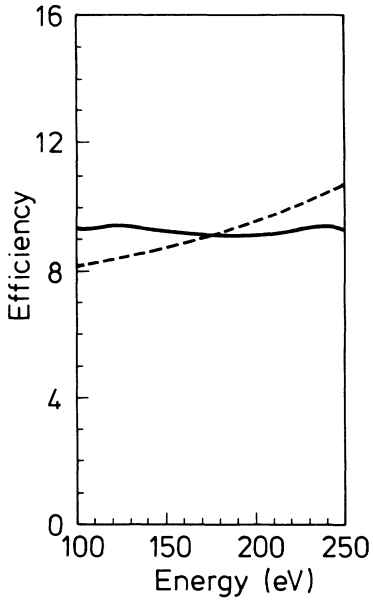

FIG. 4. Efficiency of sodium salicylate in the transmission mode as a function of the energy of the exciting radiation. The solid line is replotted from Fig. 1 of Ref. 9. The dashed line is calculated from Eq. (18) using optimized parameters (see text): layer thickness 13 μm; grain diameter 4.33 μm; absorption coefficient $s=1$ cm^{-1} and scattering coefficient $r=2.31\times10^{3}$ cm^{-1}, resulting in α equal to 68 cm^{-1} and H_{∞} equal to 0.971; diffusion length $L=50$ nm and reduced surface recombination velocity $S^{*}=0.0$.

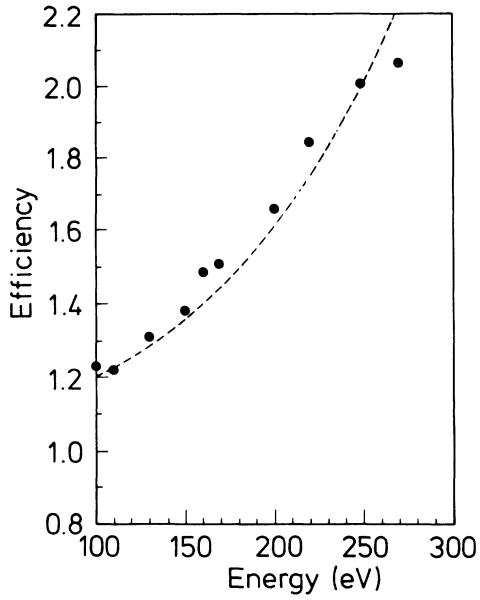

FIG. 5. Efficiency of sodium salicylate in the transmission mode as a function of the energy of the exciting radiation. The dots are replotted from Fig. 2 of Ref. 10. The dashed line is calculated from Eq. (18) using optimized parameters (see text): layer thickness 13 μm; grain diameter 2.17 μm; absorption coefficient $s=1$ cm^{-1} and scattering coefficient $r=4.61\times10^{3}$ cm^{-1}, resulting in α equal to 96 cm^{-1} and H_{∞} equal to 0.979; diffusion length $L=50$ nm and reduced surface recombination velocity $S^{*}=0.1$.

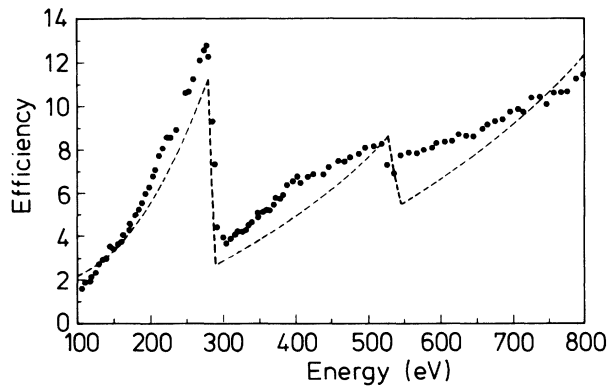

FIG. 6. Efficiency of sodium salicylate in the transmission mode as a function of the energy of the exciting radiation. The dots are replotted from Fig. 4 of Ref. 11. The dashed line is calculated from Eq. (18) using optimized parameters (see text): layer thickness 13 μm; grain diameter 0.25 μm; absorption coefficient $s=1$ cm^{-1} and scattering coefficient $r=4.0\times10^{4}$ cm^{-1}, resulting in α equal to 283 cm^{-1} and H_{∞} equal to 0.993; diffusion length $L=50$ nm and reduced surface recombination velocity $S^{*}=1000$.

negative edges can be found. A qualitative analysis for monocrystalline CaF_2 yielded an expected edge of 1% at the K edge,[8] while Bianconi *et al.*[1] found a negative edge of 4%. Therefore the experimental results from Goulon *et al.*[4] on powder samples are not in contradiction with those from Bianconi *et al.*[1] on monocrystalline samples.

B. The efficiency of sodium salicylate

In the soft-x-ray region the visible luminescence of sodium salicylate is often used to monitor the x-ray photon flux. The efficiency of sodium salicylate (in the transmission mode) between 100 and 250 eV is reported to be constant by Elango *et al.* (see Ref. 9 and Fig. 4), to increase by a factor of 1.7 by Lindle *et al.* (see Ref. 10 and Fig. 5), and to increase by a factor of 6.9 by Angel *et*

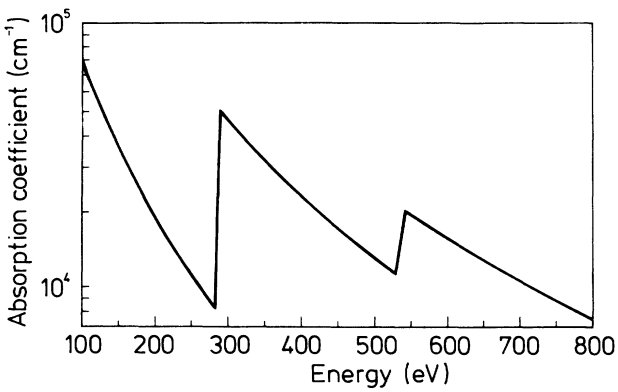

FIG. 7. Absorption coefficient of sodium salicylate as a function of the energy of the exciting radiation calculated from the data of Ref. 16. The K edges of carbon and oxygen are located at 284 and 532 eV, respectively.

(see Ref. 11 and Fig. 6). The absorption coefficient of sodium salicylate ($NaC_7H_5O_3$) calculated between 100 and 800 eV from the data of Henke *et al.*[16] is given in Fig. 7. From this figure it can be seen that in the low energy region the efficiency is most likely affected by surface recombination of the *e-h* pairs.

In an attempt to give a more quantitative interpretation of the observed differences we fitted the results of Eq. (18) to the three sets of experimental data. For the data of Angel *et al.*[11] we focused on the region below the *K* edge of carbon, as their complete set of data did not yield a unique (experimental) relation between the efficiency and the absorption coefficient (see Fig. 8). Of the parameters to be varied only the layer thickness is known to be about 13 μm for the experiments of Elango *et al.*[11] In order to minimize the numbers of adjustable parameters we kept, for all three sets, the layer thickness equal to 13 μm, the absorption coefficient s equal to 1 cm^{-1}, the scattering coefficient r equal to the inverse grain diameter, and the diffusion length L of the *e-h* pairs equal to 50 nm. The adjustable parameters left were thus the grain diameters and the reduced surface recombination velocities S^*. The results of the fits are shown in Figs. 4, 5, 6, and 8.

The good agreement between theory and experiments implies that it cannot be concluded from these experiments that the internal quantum efficiency of sodium salicylate is changing in the investigated energy range. The observed large differences in the energy dependence of the external quantum efficiency of sodium salicylate scintillators may be due to differences in starting materials and in manufacturing techniques.

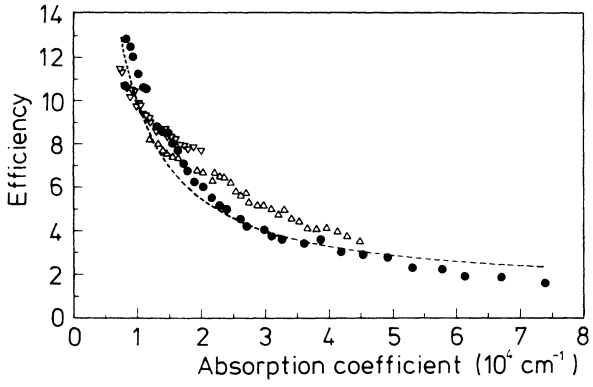

FIG. 8. Efficiency of sodium salicylate in the transmission mode as a function of the absorption coefficient of the exciting radiation replotted from Fig. 6 using the data in Fig. 7. Symbols represent the data of Angel *et al.* (Ref. 11): dots below the *K* edge of carbon; upward directed triangles between the *K* edges of carbon and oxygen; downward directed triangles above the *K* edge of oxygen. The dashed line is calculated from Eq. (18) using optimized parameters (see Fig. 6).

APPENDIX A

For a grain with boundaries at x_1 and x_2 with $x_1 < x_2$, one finds by applying the boundary condition in these points for the coefficients in Eq. (2),

$$C_1 = C_3 \frac{(S^*+1)(-S^*+\alpha L)e^{-x_1/L-\alpha x_2}+(S^*-1)(S^*+\alpha L)e^{-x_2/L-\alpha x_1}}{(S^*+1)^2 e^{(x_2-x_1)/L}-(S^*-1)^2 e^{(x_1-x_2)/L}} \tag{A1}$$

and

$$C_2 = C_3 \frac{(S^*-1)(S^*-\alpha L)e^{x_1/L-\alpha x_2}-(S^*+1)(S^*+\alpha L)e^{x_2/L-\alpha x_1}}{(S^*+1)^2 e^{(x_2-x_1)/L}-(S^*-1)^2 e^{(x_1-x_2)/L}} , \tag{A2}$$

where S^* is the reduced surface recombination velocity, i.e., the surface recombination velocity S divided by the diffusion velocity of the *e-h* pairs.

APPENDIX B

By differentiation of Eq. (5) and substitution of Eqs. (5) and (6) into this new equation one obtains

$$\frac{d^2I}{dx^2} = s(2r+s)I - \frac{2r+s}{2}P + \frac{1}{2}\frac{dP}{dx} . \tag{B1}$$

Substitution of Eqs. (7) and (8) into Eq. (B1) yields for the coefficients I_i in Eq. (8)

$$I_1 = \frac{-L^{-1}-(2r+s)}{2(L^{-2}-\alpha^2)\tau} C_1 , \tag{B2}$$

$$I_2 = \frac{L^{-1}-(2r+s)}{2(L^{-2}-\alpha^2)\tau} C_2 , \tag{B3}$$

$$I_3 = \frac{-\mu-(2r+s)}{2(\mu^2-\alpha^2)\tau} C_3 . \tag{B4}$$

By differentiation of Eq. (6) and substitution of Eqs. (5) and (6) into this new equation one obtains

$$\frac{d^2J}{dx^2} = s(2r+s)J - \frac{2r+s}{2}P - \frac{1}{2}\frac{dP}{dx} . \tag{B5}$$

Substitution of Eqs. (7) and (9) into Eq. (B5) yields for the coefficients J_i in Eq. (9),

$$J_1=\frac{L^{-1}-(2r+s)}{2(L^{-2}-\alpha^2)\tau}C_1 , \tag{B6}$$

$$J_2=\frac{-L^{-1}-(2r+s)}{2(L^{-2}-\alpha^2)\tau}C_2 , \tag{B7}$$

$$J_3=\frac{\mu-(2r+s)}{2(\mu^2-\alpha^2)\tau}C_3 . \tag{B8}$$

APPENDIX C

For a monocrystalline sample the scattering (or reemission) constant r equals zero, and consequently $\alpha=s$. This implies that instead of Eqs. (5) and (6) we have

$$\frac{dI}{dx}=-sI+\frac{P}{2} \tag{C1}$$

and

$$\frac{dJ}{dx}=sJ-\frac{P}{2} . \tag{C2}$$

The solutions of Eqs. (C1) and (C2) are given by

$$I(x)=I_-e^{-\alpha x}+I_1e^{-x/L}+I_2e^{x/L}+I_3e^{-\mu x} \tag{C3}$$

and

$$J(x)=J_+e^{\alpha x}+J_1e^{-x/L}+J_2e^{x/L}+J_3e^{-\mu x} . \tag{C4}$$

Substitution of Eq. (C3) into Eq. (C1) yields for the coefficients I_i in Eq. (C3),

$$I_1=\frac{C_1}{2(-L^{-1}+\alpha)\tau} , \tag{C5}$$

$$I_2=\frac{C_2}{2(L^{-1}+\alpha)\tau} , \tag{C6}$$

$$I_3=\frac{C_3}{2(-\mu+\alpha)\tau} . \tag{C7}$$

Substitution of Eq. (C4) into Eq. (C2) yields for the coefficients J_i in Eq. (C4),

$$J_1=\frac{C_1}{2(L^{-1}+\alpha)\tau} , \tag{C8}$$

$$J_2=\frac{C_2}{2(-L^{-1}+\alpha)\tau} , \tag{C9}$$

$$J_3=\frac{C_3}{2(\mu+\alpha)\tau} . \tag{C10}$$

The constants I_+ and I_- again are determined by the boundary conditions. Taking R as the reflection coefficient on front and back surface, these boundary conditions are: at the front surface of the sample,

$$I^{\text{front}}=RJ^{\text{front}} , \tag{C11}$$

and at the back surface of the sample,

$$J^{\text{back}}=RI^{\text{back}} . \tag{C12}$$

The optical flux from the sample in the reflection mode is now $(1-R)J^{\text{front}}$, while the optical flux in the transmission mode equals $(1-R)I^{\text{back}}$. The efficiencies of the detection process are, in the reflection mode,

$$\eta_{\text{refl}}=\frac{(1-R)J^{\text{front}}}{\mathcal{J}} , \tag{C13}$$

and in the transmission mode,

$$\eta_{\text{trans}}=\frac{(1-R)I^{\text{back}}}{\mathcal{J}} . \tag{C14}$$

[1] A. Bianconi, D. Jackson, and K. Monahan, Phys. Rev. B **17**, 2021 (1978).

[2] J. Goulon, C. Goulon-Ginet, R. Cortes, and J. M. Dubois, J. Phys. **43**, 539 (1982).

[3] J. Goulon, P. Tola, M. Lemonnier, and J. Dexpert-Ghys, Chem. Phys. **78**, 347 (1983).

[4] J. Goulon, P. Tola, J. C. Brochon, M. Lemonnier, J. Dexpert-Ghys, and R. Guillard, *EXAFS and Near Edge Structure III*, Vol. 2 of *Springer Proceedings in Physics*, edited by K. O. Hodgson, B. Hedman, and J. E. Penner-Hahn (Springer-Verlag, Berlin, 1984), p. 490.

[5] R. F. Pettifer and A. J. Bourdillon, J. Phys. C **20**, 329 (1987).

[6] J. Jaklevic, J. A. Kirby, M. P. Klein, A. S. Robertson, G. S. Brown, and P. Eisenberger, Solid State Commun. **23**, 679 (1977).

[7] J. H. Beaumont, A. J. Bourdillon, and M. N. Kabler, J. Phys. C **9**, 2961 (1976).

[8] D. B. M. Klaassen, C. M. G. van Leuken, and K. M. H. Maessen, Phys. Rev. B **36**, 4407 (1987).

[9] M. Elango, J. Pruulmann, and A. P. Zhurakovskii, Phys. Status Solidi B **115**, 399 (1983).

[10] D. W. Lindle, T. A. Ferret, P. A. Heimann, and D. A. Shirley, Phys. Rev. B **34**, 1131 (1986).

[11] G. C. Angel, J. A. R. Samson, and G. Williams, Appl. Opt. **25**, 3312 (1986).

[12] H. B. DeVore, Phys. Rev. **102**, 86 (1956).

[13] P. Kubelka and F. Munk, Z. Tech. Phys. **12**, 593 (1931).

[14] H. C. Hamaker, Phillips Res. Rep. **2**, 55 (1947).

[15] A. Bril and H. A. Klasens, Philips Res. Rep. **7**, 401 (1952).

[16] B. L. Henke, in *Low Energy X-Ray Diagnostics, Monterey, 1981*, Proceedings of the Conference on Low Energy X-Ray Diagnostics, AIP Conf. Proc. No. 75, edited by D. T. Attwood and B. L. Henke (AIP, New York, 1981), p. 146; B. L. Henke, P. Lee, T. J. Tanaka, R. L. Shimabukuro, and B. K. Fujikawa, *ibid.*, p. 340; B. L. Henke, P. Lee, T. J. Tanaka, R. L. Shimabukuro, and B. K. Fujikawa, At. Data Nucl. Data Tables **27**, 1 (1982).